Major *et al. Geotherm Energy (2018) 6:1*
https://doi.org/10.1186/s40517-018-0089-0

Geothermal Energy

RESEARCH Open Access

# A numerical investigation of combined heat storage and extraction in deep geothermal reservoirs

Márton Major[1*], Søren Erbs Poulsen[2] and Niels Balling[1]

*Correspondence: marton.major@geo.au.dk
[1] Department of Geoscience, Aarhus University, Aarhus, Denmark
Full list of author information is available at the end of the article

**Abstract**

Heat storage capabilities of deep sedimentary geothermal reservoirs are evaluated through numerical model simulations. We combine storage with heat extraction in a doublet well system when storage phases are restricted to summer months. The effects of stored volume and annual repetition on energy recovery are investigated. Recovery factors are evaluated for several different model setups and we find that storing 90 °C water at 2500 m depth is capable of reproducing, on average 67% of the stored energy. In addition, ambient reservoir temperature of 75 °C is slightly elevated leading to increased efficiency. Additional simulations concerning pressure build-up in the reservoir are carried out to show that safety levels may not be reached. Reservoir characteristics are inspired by Danish geothermal conditions, but results are assumed to have more general validity. Thus, deep sedimentary reservoirs of suitable properties are found to be viable options for storing access energy for high-demand periods.

**Keywords:** Heat storage, Recovery, Numerical modelling, Geothermal energy, Deep sedimentary reservoirs

## Introduction

Using sedimentary reservoirs for thermal energy storage is a concept that has been around for decades (Molz et al. 1978; Carotenuto et al. 1991; Kim et al. 2010; Drijver et al. 2012; Sommer et al. 2014) and is gaining more attention as the share of renewable energy use is increasing worldwide (REN21 2017). Increasing the efficiency and sustainability of such systems could save precious natural resources. Reservoirs at different depths have been tested and modelled with various setups to improve efficiency. For example, Molz et al. (1978) ran tests on short-term storage of 36 °C water in a confined aquifer near Mobile, Alabama, USA, and calculated a recovery factor of 0.69. More recently, Drijver et al. (2012) found that storing 93 °C water at medium depth (600–700 m) was capable of up to 80% recovery efficiency in some cases.

Shallow aquifers are widely used for storing access energy produced by solar panels for the winter months, as is with the German Parliament in Berlin for example, where an underground storage system has been operational since 2002 (Sanner et al. 2005). These shallow systems are capable of aiding district heating systems, but sometimes strict regulations prohibit the injection of high-temperature water, due to environmental

concerns and potential contamination of drinking water (Welsch et al. 2015). Storing higher temperatures in shallow depths is also less efficient because of higher energy loss, due to larger temperature gradients. For these reasons, it makes sense to investigate the possibility of storing high-temperature water at medium and even high depths (Welsch et al. 2015).

Many studies have contemplated the effectiveness of different borehole arrangements to maximize productivity from deep sedimentary reservoirs. An early study by Gringarten (1978) showed that using so-called doublet well systems combining production and reinjection increases reservoir lifetime and helps in heat recovery. He also found that combining precisely placed doublets will increase productivity and sustainability. Doublet systems are a standard for geothermal production today and are in use worldwide with many different borehole arrangements.

In Denmark sedimentary formations at 1000–3000 m depth, such as the Bunter sandstone and Gassum formations, are utilized for district heating purposes in three locations (Røgen et al. 2015; Mahler and Magtengaard 2010). Our goal is to investigate storage capabilities of such a deep sedimentary reservoir representing characteristic deep geothermal conditions, through a series of numerical models. Whilst shallow reservoir applications are well understood, much less work has been done on deep sedimentary reservoirs, especially combining storage and production. This study aims at narrowing the knowledge gap between deep and shallow systems. We are using a single doublet system with combined production and reinjection, where 90 °C water is stored via reversed flow during the summer months. All subsequent models are run in FEFLOW groundwater-flow simulation software.

## Theory

To accurately represent real-life conditions, the modelling software, FEFLOW solves three sets of equations. The standard flow equation for a confined aquifer with a groundwater source (Diersch 2009):

$$Q = S_s \frac{\partial h}{\partial t} + \nabla \boldsymbol{q} \tag{1}$$

where $Q$ is the volumetric source rate per unit volume, $S_s$ is the specific storage, $h$ is the hydraulic head, and $\boldsymbol{q}$ is the Darcy velocity. Since both viscosity and density are temperature-dependent parameters, and the Darcy velocity ($\boldsymbol{q}$) is dependent on them; the formulation of the Darcy equation according to Diersch (2009) becomes:

$$\boldsymbol{q} = -\boldsymbol{K} f_\mu \left( \nabla h + \frac{\rho_f - \rho_0}{\rho_0} \boldsymbol{e} \right) \tag{2}$$

where $\boldsymbol{K}$ is the hydraulic conductivity tensor, $f_\mu$ is the ratio of reference viscosity to dynamic viscosity, $h$ is the hydraulic head, $\rho_f$ and $\rho_0$ are the fluid and reference density, respectively, and $\boldsymbol{e}$ is the gravitational unit vector.

Finally, the density coupled heat equation solved in FEFLOW, taking into account thermal dispersion, according to Diersch (2009) is:

$$(\rho c)_b \frac{\partial T}{\partial t} = \nabla \cdot \left[ \left( \lambda_b \mathbf{I} + (\rho c)_b \mathbf{D} \right) \cdot \nabla T \right] - (\rho c)_f \mathbf{q} \cdot \nabla T + H \tag{3}$$

where $(\rho c)_b$ and $(\rho c)_f$ are the bulk and fluid volumetric heat capacity, respectively, $\lambda_b$ is the bulk thermal conductivity (the arithmetic mean of fluid and matrix conductivity in this case, weighted according to porosity), **I** is the unit tensor, **D** is the tensor of mechanical dispersion, and $H$ is the bulk heat sink/source. Equations 1, 2, and 3 are solved in three dimensions using Galerkin's version of the finite element method.

## Model setup

The following chapter details the specific setup of the starting model, which was based on Poulsen et al. (2015) and formulated by Major (2016) with the exception of the "Recovery factor" section. Specific parameters were chosen to represent similar conditions to that of the Margretheholm geothermal plant currently operated in the Copenhagen area. This in particular applies to reservoir depth, well distance, and reservoir temperatures (cf. Røgen et al. 2015).

### Model area

The conceptual model extends 10 km × 10 km horizontally and 1050 m in the vertical direction (Fig. 1). The reservoir is represented by a 50-m-thick permeable layer, which is bounded by two identical 500-m-thick impermeable confining beds. The finite element mesh is generated using FEFLOW's automatic mesh generator with triangular elements. The production and injection wells (referred to as P1 and I1 from here on) are located 1200 m apart at ($x = 5000$, $y = 4400$) and ($x = 5000$, $y = 5600$), respectively. The top of the model was set to − 2000 m depth resulting in the reservoir extending from − 2500 to − 2550 m depth, which roughly corresponds to the location of the Bunter sandstone formation used for district heating near Copenhagen (Røgen et al. 2015; Mahler and Magtengaard 2010). Detailed explanation on the geological setting at the Margretheholm plant is presented in Fig. 9 of Poulsen et al. (2015).

### Spatial discretization

Elements around the wells are refined to ensure numerical stability. This is achieved by building the well locations and supporting nodes around them directly into the mesh.

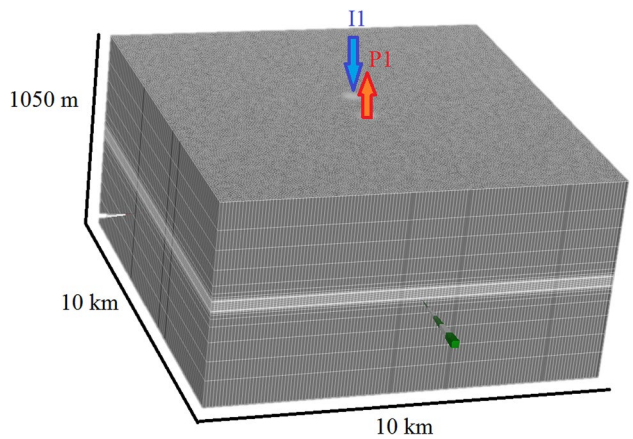


**Fig. 1** Model domain after spatial discretization and refinement. P1 denoting the production well and I1 the injection well

The supporting nodes are located at a given distance (Δ) from the wells to optimize mesh refinement, which was determined based on the formula by Diersch et al. (2011):

$$\Delta = ar_b \tag{4}$$

where $r_b$ is the borehole radius, and $a$ is a constant dependent on the number of nodes. In this case, we used six supporting nodes for each borehole which is a common standard for triangular, horizontal meshes (Diersch et al. 2011). This resulted in a value of $a = 6.13$ according to Diersch et al. (2011), and gave the ideal distance for these nodes to be 0.613 m, corresponding to the chosen 0.1 m borehole radius.

Numerical stability is measured by the Peclét number (*Pe*). Since in this model, the overwhelming fluid-flow direction is perpendicular to the heat flow and longitudinal dispersion and mixing dominates, then according to Voss and Provost (2003):

$$Pe \approx \frac{\Delta L}{\alpha_L} \tag{5}$$

where $\Delta L$ is the distance between model nodes and $\alpha_L$ is the longitudinal thermal dispersivity. $Pe < 2$ guarantees stability.

For reasons above, vertical discretization of both the reservoir and the confining beds is also implemented by subdividing them into multiple layers. Minimum layer thickness is 0.5 m and is gradually increased away from the aquifer–aquitard boundary to 140 m in the confining beds and 5 m in the reservoir. After refinement, the base model consists of 37 slices and 36 layers, respectively, and has more than 900 thousand nodes and 1.75 million elements.

#### Model parameters

Fluid density is set to 1170 kg/m$^3$, which corresponds to a 20 w% NaCl brine at 20 °C (Mahler and Magtengaard 2010) and controlled via the reference density option in FEFLOW. Hydraulic conductivity of the reservoir is set to $4 \times 10^{-6}$ m/s, which corresponds to 0.5 Darcy in permeability. Conductivity of the confining beds is $10^{-11}$ m/s for clay-rich rock of low permeability (Dominico and Schwartz 1998). Specific storage can be calculated from porosity and compressibility values of water and rock, based on Schwartz and Zhang (2003), and gives $2 \times 10^{-6}$/m in this case.

Through the entire model, porosity is set to 25% based on Mathiesen et al. (2009). Thermal conductivity of the fluid is slightly lower than fresh water at 0.62 W/m/°K, as salinity decreases conductivity (Phillips et al. 1981). Matrix conductivity is set to 2.0 and 6.0 W/m/°K in the confining beds and the sandstone reservoir, respectively (Robertson 1988). Volumetric heat capacity of the pore fluid is 4.0 MJ/m$^3$/°K (Phillips et al. 1981) and matrix heat capacity is 2.3 MJ/m$^3$/°K for both the reservoir and the beds (Chesworth 2008; Robertson 1988). Thermal dispersivity is set to 10 m in the longitudinal and 1 m in the transverse direction, which we deemed appropriate for the given length scale based on Gelhar et al. (1992). Low values can also lead to numerical instability. Typically transverse dispersivity is an order of magnitude smaller than longitudinal dispersivity (Gelhar et al. 1992). Model parameters are listed in Table 1.

Although this model attempts to simulate real conditions, several simplifications and assumptions are made. First of all, homogeneity is assumed for both the reservoir and

**Table 1 Model thermal and hydraulic parameters**

| Parameter | Reservoir | Confining bed |
|---|---|---|
| Thickness (m) | 50 | 500 |
| Hydraulic conductivity (m/s) | $4 \times 10^{-6}$ | $10^{-11}$ |
| Specific storage (1/m) | $2 \times 10^{-6}$ | $2 \times 10^{-6}$ |
| Thermal conductivity of matrix (W/m/°K) | 6.0 | 2.0 |
| Thermal conductivity of fluid (W/m/°K) | 0.62 | 0.62 |
| Volumetric heat capacity of matrix (MJ/m$^3$/°K) | 2.3 | 2.3 |
| Volumetric heat capacity of fluid (MJ/m$^3$/°K) | 4.0 | 4.0 |
| Longitudinal dispersivity (m) | 10 | 10 |
| Transverse dispersivity (m) | 1 | 1 |
| Porosity (%) | 25 | 25 |

the confining beds. This is not met in natural environments and inhomogeneity may have significant impact on efficiency and sustainability. Same can be said of anisotropy, not considered. Such complexities may typically be related to local conditions and are difficult to measure and thus not included here. Present study has a more general aim.

#### Boundary conditions

Horizontally, the model ends in thermal and hydraulic no-flow boundaries. The upper model boundary is represented by a constant temperature of 55 °C and hydraulic head of 0 m, whereas the lower boundary has a background heat flow of 65 mW/m$^2$ (typical value for sedimentary basins in north-western Europe, Balling, 1995), and no fluid flow across. The temperature of the upper boundary is calculated assuming surface temperature of 8 °C and thermal gradient of 23.5 °C/km which is within the range of average Danish values (Balling et al. 2016). Both wells are represented by highly conductive 1D elements, and their properties are controlled via the Multilayer Well Boundary conditions. This means, that heat flow in the wells is strictly vertical and no heat loss to the confining units is assumed.

Flow rates of the wells are set equal to 3600 m$^3$/day and injection temperature is set to 20 °C at the reservoir. Initial temperature and hydraulic head distribution is given by a steady-state model simulation with the above conditions, and no pumping. Steady-state simulation yields an average reservoir temperature of 75 °C, which will serve as the initial production temperature for all subsequent transient simulations.

#### Recovery factor

In this study, we evaluate the efficiency of the proposed system via a recovery factor. Our definition of the recovery is similar to that of previous studies (e.g. Molz et al. 1978; Drijver et al. 2012; Sommer et al. 2014; Schout et al. 2014). It is evaluated as the ratio of recovered energy to the stored energy, with respect to ambient reservoir temperature and with equal volume of water stored and produced. Our reasoning behind using this method, besides allowing us to compare results to previous studies, is the better understanding of loss processes. Calculating recovery with respect to cold well temperature was considered and eventually carried out for some of our simulations, but these values were discarded due to a rather complex representation of the system. In these scenarios,

water temperature increases when pumped up during storage phases, due in part to high ambient temperatures in the reservoir. This means that stored energy would be compared to higher temperatures than the extracted energy, which would result in serious positive bias towards recovery estimation. In some cases, we get recoveries as high as 115%. Values this high obviously do not represent subsurface physical processes and do not allow us to see if any losses occurred during the storage cycle. Additionally, these values are highly dependent on the thermal history of the reservoir, meaning the initially available cold water volume.

## Comparative study

As a first step, a 300-year simulation was carried out, with production from P1 and reinjection of 20 °C water in I1, to study the evolution of the simple geothermal system and to be able to validate the model by comparison to the results of Poulsen et al. (2015). Although it may not be realistic to expect 300 years of operation from a plant, our goal in this simulation is merely to demonstrate long-term reservoir temperature evolution.

Figure 2 shows the temperature profile in the P1 well at the reservoir level over this 300-year period. The curve can be divided into two sections based on overall characteristics. The first 30 years show steady production temperatures of about 75 °C before

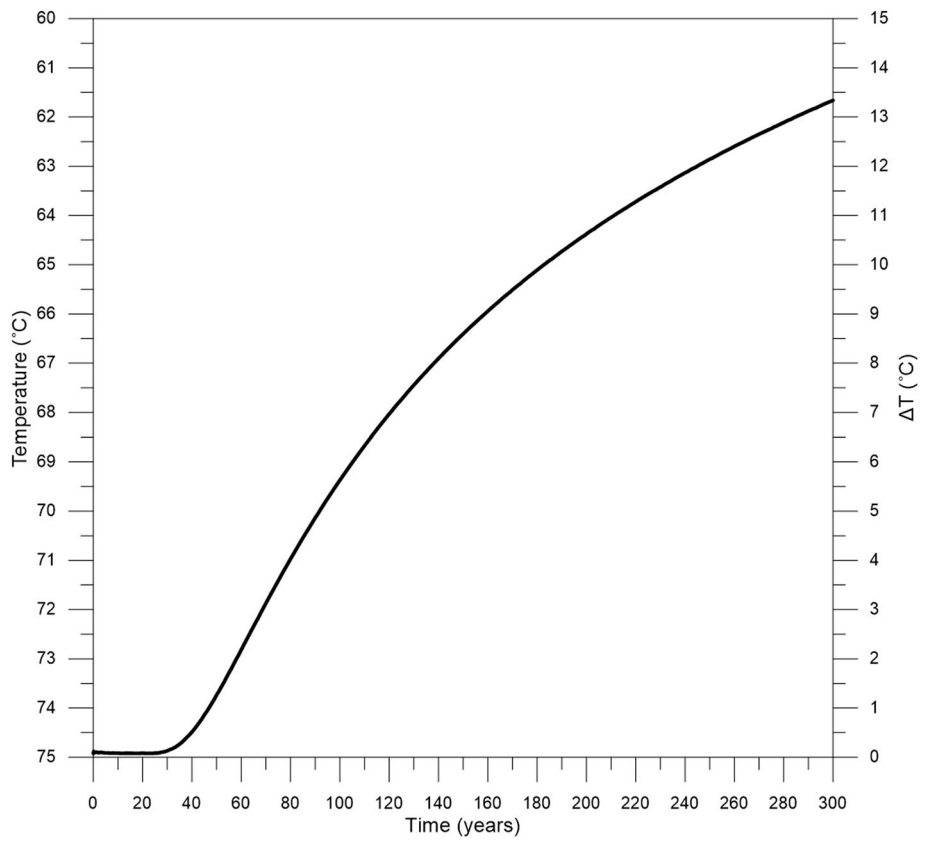


**Fig. 2** Temperature profile at the reservoir level in P1 during a 300-year model simulation with combined production and reinjection

thermal breakthrough initiates the continuous declining phase. After 300 years, the temperature decreases to about 61.7 °C, which is a − 13.2 °C change compared to the starting temperature. These results agree with the findings of Poulsen et al. (2015) within 5% accuracy.

Such minor differences can be explained by the nuances in model setup such as meshing density and smoothness, as well as time-stepping conditions during simulation runs, which may not have been identical between the two simulations.

## Conceptual models

Storage simulations were run for the described model, where 90 °C water is stored in the reservoir during the summer months, by way of reversing the doublet. The idea is based on the possibility of multi-doublet systems operating at reduced capacity during times of lower energy demand (i.e. summertime). Over time, these storage periods would increase productivity when more energy is required (i.e. winter).

Our goal is to evaluate the recovery efficiency of the stored energy when both storage and simulation times are varied. The efficiency of the system is assessed via the recovery factor described in the "Recovery factor" section. Injection times are set to 1, 2, 3 and 4 months, corresponding to June, June–July, June–August and June–September in terms of time of year. Obviously, longer injection time results in more surplus energy stored and promises higher production temperatures for the winter months.

Processes affecting recovery efficiency were detailed by Doughty et al. (1982). These include thermal conduction, dispersion, regional groundwater flow and the properties of the reservoir. Recently, much emphasis has been put on evaluating the effect of density-driven flow or buoyancy flow on recovery (Drijver et al. 2012; Schout et al. 2014). These factors should be kept in mind when evaluating results.

In all subsequent models, simulation times are significantly shorter than in the base model to reduce computation time. Reversing the flow in the doublet requires reduced time-stepping settings which in turn increases computation time drastically. Nevertheless, the effects of summertime storage should be evaluated in the long term as well. Expectations are that repeated use of summer injection will increase reservoir lifetime and efficiency over long time periods (Drijver et al. 2012). Simulation times were set to cover 1, 3 and 10 storage cycles which correspond to 1.4, 3.4 and 10.4 years, respectively.

Some additional simulations were carried out to examine pressure build-up in the reservoir during operation. Safety regulations are in place at every plant in Denmark to ensure secure operation. Surface installations may be designed to operate up to 100 bar = 10,000 kPa of pressure, but often a lower limit of 7000–7400 kPa is used in practice (Allan Mahler, personal communication). At the surface hydrostatic pressure is zero, and in all simulations pressure values are from the reservoir level. Therefore, only the change in pressure is relevant and—assuming even distribution with depth—it can be projected to the surface.

The evolution of pressure conditions in the reservoir was tested through two additional simulations. At first, a 10-year simulation was carried out, when the I1 well was shut down for the storage periods, thus adding extra water volume to the system. The second simulation was a 20-year experiment, where water is continuously injected into

P1 without production from I1 to see how long it takes to reach the aforementioned safety levels. Table 2 summarizes the different time settings used in simulations.

## Results and discussion

### Storage time

Four separate simulations were run with storage times of 1, 2, 3, and 4 months. During these periods, 90 °C water was injected into P1 with a rate of 3600 $m^3$/day for each simulation and running time was 1.4 years in all cases. Results are presented in Fig. 3.

Significant difference in temperature decline is apparent between the models. After 1.4 years, the production temperature only increases about 0.1 °C in the case of June

**Table 2 Summary of time frame values used for storage simulations**

| **Storage time** | 1 month | 2 months | 3 months | 4 months |
|---|---|---|---|---|
| **Simulation time** | 1.4 years | 3.4 years | 10.4 years | |
| **Pressure** | 10 years of summertime storage | 20 years of continuous injection | | |

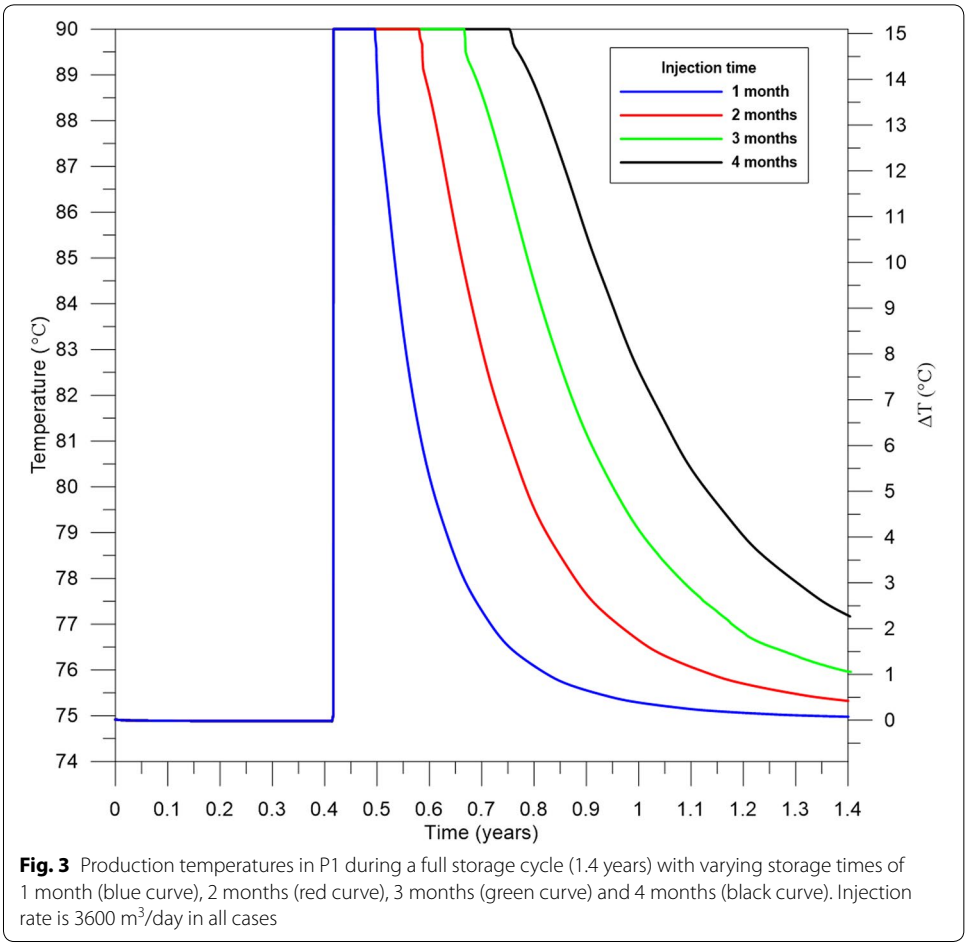


**Fig. 3** Production temperatures in P1 during a full storage cycle (1.4 years) with varying storage times of 1 month (blue curve), 2 months (red curve), 3 months (green curve) and 4 months (black curve). Injection rate is 3600 $m^3$/day in all cases

injection (blue curve), whereas injection throughout September (black curve) generates about 2.3 °C warmer temperatures than before the storage phase. This difference corresponds to a 9.2 MWh increase in energy production at the end of the storage cycle. Using 2 and 3 months of injection (red and green curves) creates a 0.4 and 1.0 °C increase in production temperature after one cycle. These results highlight the benefit of using longer storage periods to gain more energy in the winter. However, in most cases geothermal plants may heavily be relied on also during summer, thus preventing prolonged storage phases.

Figure 4 shows how much of the stored energy is recovered during the pumping period. Recovery factors are calculated with respect to equal volume as mentioned before, which means the 1-month storage phase is evaluated through 30 days of production (blue curve), 2-month storage during a 61-day production phase (red curve), 3-month storage for a 92-day period (green curve) and the same way with a 4-month storage period, which is evaluated during a 123-day interval (black curve). As mentioned before, boreholes are assumed to have strictly 1D flow and losses through the borehole sides are ignored. This means that recovery factors can be considered to be valid at the surface. Shorter storage time results in faster energy recovery as seen from the steepness

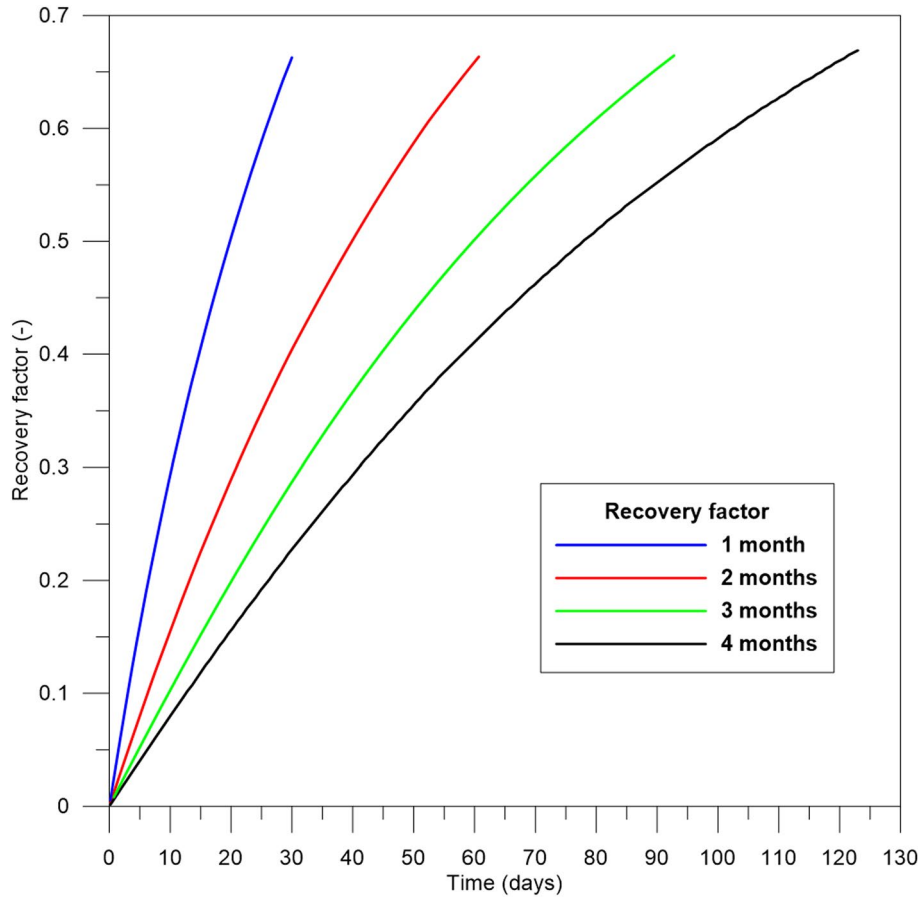


**Fig. 4** Recovery factors for varying storage phases of 1 month (blue curve), 2 months (red curve), 3 months (green curve) and 4 months (black curve). Values are normalized to total surplus energy stored during storage phase

of the curves (Fig. 4). This makes sense, since less energy is injected in a shorter time span, so heat losses to the other layers through conduction, convection, and dispersion will not be as significant as with longer storage periods. After 30, 61, 92, and 123 days of production, recovery factors are 66, 67, 67, and 67%, respectively. These results are in accordance with findings of earlier studies (Molz et al. 1978; Drijver et al. 2012; Sommer et al. 2014). Recovering two-thirds of the stored energy promises high-temperature deep storage to be beneficial, but we should keep in mind that losses through the borehole walls are ignored in these simulations.

Also important to note that the curves are normalized to the surplus stored energy during each time interval. Meaning, the total produced energy is, of course, more after a 4-month storage period than in the other two cases. Total surplus energy production during each recovery phase in these four cases is 2389, 4167, 5500, and 6667 MWh, respectively. This is a 174, 230, and 279% increase in energy production for 2, 3, and 4 months of storage phases compared to 1-month injection.

Figure 5 shows no evidence of the 20 °C injected water during heat extraction having any influence on production temperature during these simulations. This is expected, since the base simulation indicated the temperature breakthrough time to be over 30 years for a similar model setup. The stored 90 °C temperature front coupled with the cold water being pumped out during storage periods is expected to keep away the cold front even longer in storage simulations, so the cold water will only have an effect after long-term operation, if at all. This result highlights the advantage of a combined system in delaying breakthrough times, which in turn provides the possibility of reduced well spacing without compromising on sustainability.

### Simulation time

So far, simulation times were set to 1.4 years in each case due to computation limitations detailed above. However, long-term effects should always be investigated, as they may indicate unforeseen trends. Therefore, additional simulations of 3.4 (3 cycles) and 10.4 years (10 cycles) were carried out, where storage time was set to 3 months and

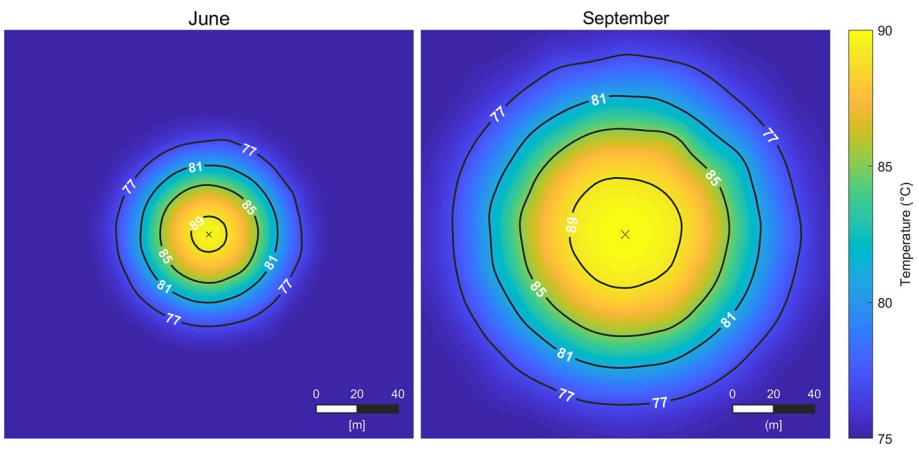


**Fig. 5** Contour plot of affected area by 90 °C injection; after a 1-month storage period (left); after a 4-month storage period (right)

injection rate to 3600 $m^3$/day. Results of the 3- and 10-cycle simulation with annual 3-month storage of 90 °C water are shown in Fig. 6. After 1 cycle, production temperature increases 1.0 °C. After the second storage cycle, reservoir temperatures increase further by an additional 0.25 °C. The rate of increase slows down further leading to a mere 0.1 °C growth at the end of the third cycle. Altogether, we experience about a 1.35–1.4 °C temperature increase within the simulated 3.4-year period.

An important feature of the system is production temperatures staying above the initial values, meaning that the stored 90 °C water constantly keeps warming up the reservoir around the P1 well. This means elevated energy production for the entire storage cycle. The slowing rate of increase indicates that the reservoir is approaching a steady, elevated temperature which is maintained by the annual storage phase and could potentially go on for decades, barring pressure increase above safety limits and potential interference from the cold water front.

These results warrant the study of longer simulations to see potential effects that have not been impacting results so far. A 10.4-year simulation of the same setup was carried out for this exact purpose and results are shown in Fig. 6.

Reservoir temperature increase is minuscule after 3 cycles and production temperature settles around 76.4 °C, which is 1.5 °C higher than in the beginning. This ambient temperature is then maintained throughout the simulation until the end of the 10th cycle. Based on these results, we can see no significant losses occurring in the reservoir, and the cold water front from I1 apparently has no effect on production temperature. Buoyancy flow does not seem to be a factor, most likely due to the small difference

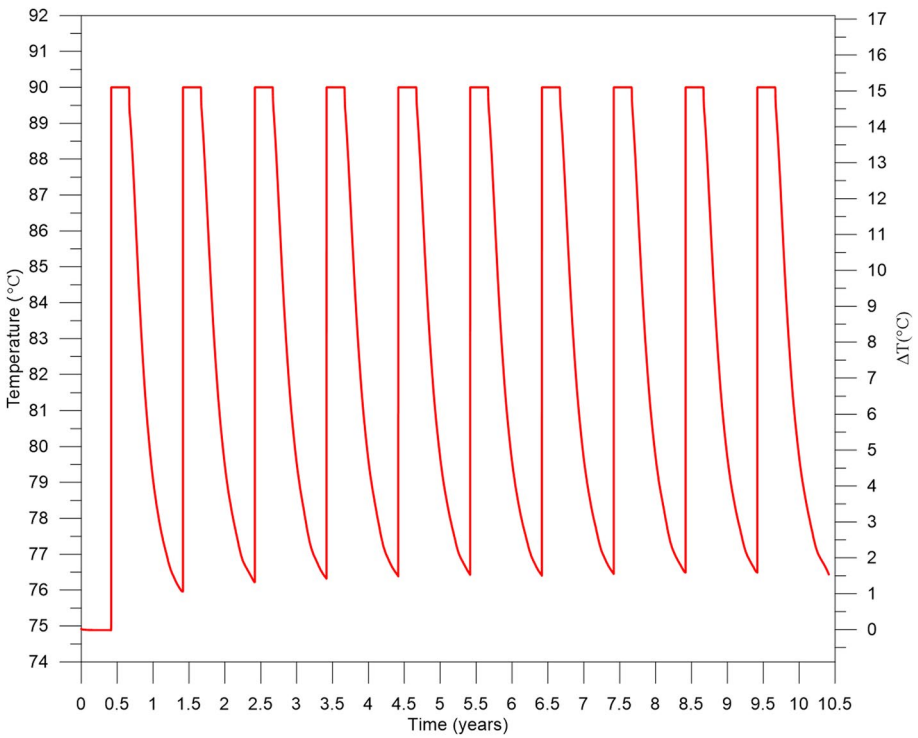


**Fig. 6** Temperature history in P1 during a 10.4-year simulation with annual storage phase of 3 months

in reservoir and injection temperature. This suggests that the energy recovery might improve after several years of operation as was the case for Drijver et al. (2012). Compared to their findings of close to 20% increase in recovery efficiency, however, our model only produces a mere 1% more energy in the 10th year of operation than in the first year.

The reason behind this big difference is most likely the smaller temperature gradient in our setup, due to high ambient reservoir temperatures at large depths. Drijver et al. (2012) ran their model for an aquifer at medium depth (700 m) with a temperature difference of 42 °C between injected and reservoir temperature, which is significantly larger than the 15 °C difference used in our models.

### Pressure

Pressure history in P1 during 10 years of operation is shown on Fig. 7, when I1 was shut down for storage periods. As apparent from the figure, pressure is increasing annually, but the rate of increase seems to slow down after 5–6 years of operation. From the 9th to 10th year, it is only about a 50 kPa increase compared to 100 kPa seen in the first 3 years annually. With these declining rates, the implications are that such a system could also stay effective during long-term operation.

The 20-year continuous injection test shows pressure levels in both wells (Fig. 8). An overall increasing trend is obvious and the rate of increase is close to identical for the two wells. P1 reaches about 7300 kPa after 20 years, which is right around the safety limit used in practice. Based on these results, we can safely say that pressures should not reach dangerous levels even with long-term repeated use of summer storage. Important

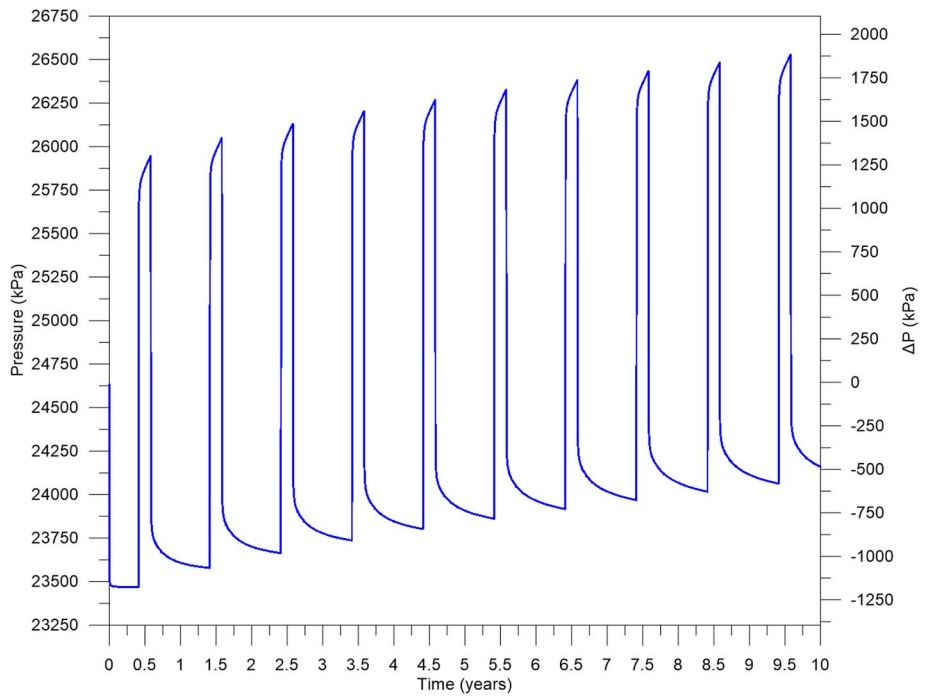


**Fig. 7** Pressure history in P1 during a 10-year simulation with annual storage phase of 2 months when I1 was shut down

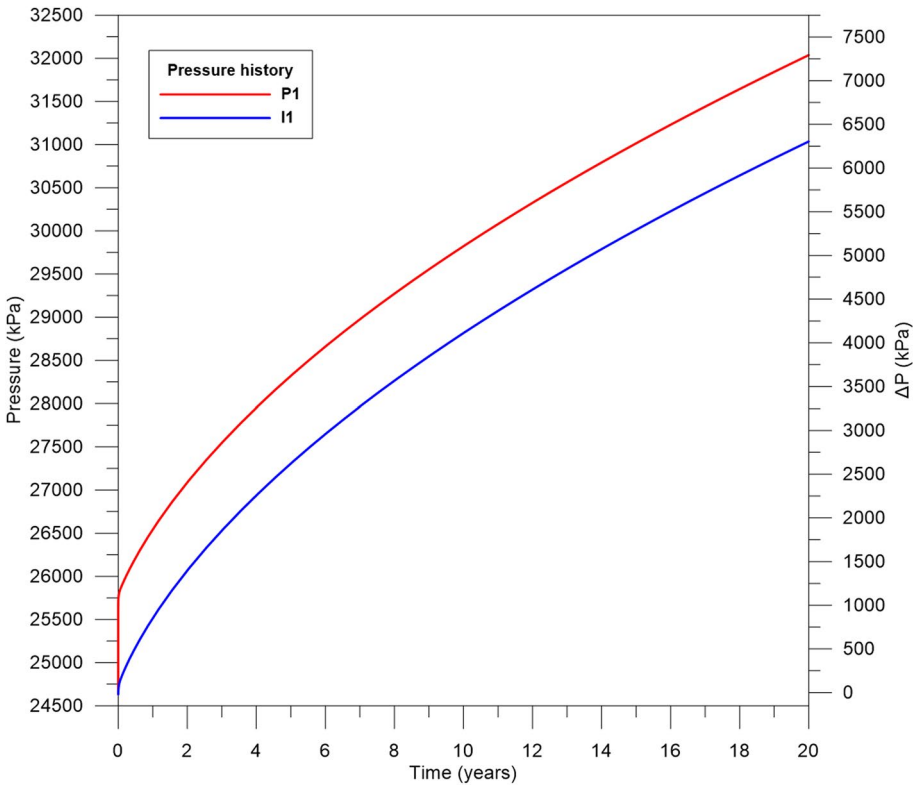


**Fig. 8** Pressure history of constant injection with a rate of 3600 $m^3$/day and no production during 20 years. Red curve represents P1 and blue curve represents I1

to note, however, that technical and chemical factors, such as clogging and condensation on the filters, can significantly increase the required injection pressure.

## Summary and conclusions

Simulations concerning annual storage of high-temperature water were carried out on a single doublet system, and the effects of injection time and long-term simulation were evaluated.

Injecting 90 °C water resulted in increased reservoir temperature for the rest of the year. Annual storage phases of 1, 2, 3, and 4 months all generated 67% recovery on average, which are similar to findings of other researchers (Molz et al. 1978; Drijver et al. 2012; Sommer et al. 2014).

Simulating multiple cycles of operation allowed us to evaluate long-term behaviour and make educated guesses towards the future. Production temperature stays above the steady-state starting temperature after 10.4 years of operation, and slightly increases year by year. Recovery factor does increase about 1% after 10 cycles, but does not confirm the close to 20% increase found by Drijver et al. (2012). This difference is most likely due to the difference in aquifer depth, which is close to 2000 m deeper in our simulations. Deep aquifers ensure high temperatures, resulting in lower gradient between injected and reservoir water temperature limiting the rate of conductive heat loss and the effect of buoyancy flow.

In conclusion, deep storage at high temperatures seems a viable option for harvesting access heat energy. If geothermal plants can operate on limited capacity during summer, storage can help immensely in increasing productivity the rest of the year when heating demand is generally significantly higher. Aquifers at large depths have the advantage of limited losses and thermal recharge from large confining volumes. An average recovery factor of 67% is very reasonable and may be worth the investment. An added incentive of using such systems is the reduced environmental concerns limiting high-temperature storage at shallow depths. Reinjecting the water pumped out from the reservoir itself results in injection water of similar chemical composition. In addition, delayed breakthrough times caused by annual storage give an opportunity to reduce well spacing and not compromise on sustainability. Pressure simulations also showed that reaching safety limits should not be a concern, unless scaling, clogging and other technical difficulties arise.

Using thermal storage for load balancing of solar district heating systems is a practical solution which has been implemented in Brædstrup, Denmark for example, and proved to be an effective method for evening out base load during the year (Tordrup et al. 2016). Converting wind turbine currents to thermal energy for storage purposes is also a method which is gaining more attention to eliminate wind power variability (Atherton et al. 2017). Although these systems do not yet utilize deep sedimentary reservoirs for thermal storage, we believe a better understanding of deep storage processes can provide an alternative to current techniques.

Numerical models representing realistic sediment composition and anisotropy of thermal and hydraulic parameters could give valuable additional information on loss processes, as well as more accurate projections for sustainability. In particular, losses through the sides of boreholes should be of interest in future simulations.

Technical difficulties, such as the clogging of well screens and well design, were not accounted for in our models, but can have serious effects in real-life applications. Projecting the clogging and potential corrosion of well screens based on solute composition of reservoir fluid would help with planning future investments. The performance of a multi-doublet system, where one or more of the doublets are used for storage during limited operation periods, could also be of interest in later studies.

**Abbreviations**

I1: injection well; P1: production well.

**Authors' contributions**

MM built the models discussed and ran all simulations as well as drafted the manuscript as part of his Ph.D. studies with elements from his Master's thesis. SEP built the model based on which the comparative model was constructed, provided parameters used in the conceptual model, as well as significant experience with FEFLOW modelling. NB, as project supervisor, designed main elements of this study, provided guidance and insight in evaluating the results and helped draft the manuscript. All authors read and approved the final manuscript.

**Author details**

[1] Department of Geoscience, Aarhus University, Aarhus, Denmark. [2] Centre for Applied Research and Development, VIA University College, Horsens, Denmark.

**Acknowledgements**

Parts of this study were financially supported by Innovation Fund Denmark in project GEOTHERM—Geothermal energy from sedimentary reservoirs—Removing obstacles for large scale utilization.

**Competing interests**

The authors declare that they have no competing interests.

**Availability of data and materials**
All relevant data and material are presented in the main paper.

**Consent for publication**
Not applicable.

**Ethics approval and consent to participate**
Not applicable.

## Publisher's Note



Received: 14 July 2017 Accepted: 9 January 2018
Published online: 19 January 2018

**References**

Atherton J, Sharma R, Salgado J. Techno-economic analysis of energy storage systems for application in wind farms. Energy. 2017;135:540–52.
Balling N. Heat flow and thermal structure of the lithosphere across the Baltic Shield and northern Tornquist Zone. Tectonophysics. 1995;244(1–3):13–50.
Balling N, Poulsen SE, Fuchs S, Mathiesen A, Bording TS, Nielsen SB, Nielsen LH. Development of a numerical 3D geothermal model for Denmark. Strasbourg: Proc Eur Geotherm Congr; 2016. p. 19–24.
Carotenuto A, Fucci F, La Fianza G, Reale F. Physical model and demonstration of an aquifer thermal energy store. Heat Recover Syst CHP. 1991;11(2–3):169–80.
Chesworth W, editor. Encyclopedia of soil science. Dordrecht: Springer; 2008. p. 902.
Diersch H-JG. FEFLOW reference manual. Berlin: WASY Gmbh, Institute for Water Resources Planning and Systems Research; 2009.
Diersch H-JG, Bauer D, Heidemann W, Rühaak W, Schätzl P. Finite element modelling of borehole heat exchanger systems part 2: numerical simulation. Comput Geosci. 2011;37:1136–47.
Dominico PA, Schwartz FW. Physical and chemical hydrology. New York: Wiley; 1998. p. 506.
Doughty C, Hellström G, Tsang CF, Claesson J. A dimensionless parameter approach to the thermal behaviour of an aquifer thermal energy storage system. Water Resour Res. 1982;18(3):571–87.
Drijver B, Aarssen MV, Zwart B. High-temperature Aquifer thermal energy storage (ATES): sustainable and multi-usable. Paper presented at Innostock. 2012.
Gelhar L, Welty C, Rehfeldt KR. A critical review on field-scale dispersion in aquifers. Water Resour Res. 1992;28(7):1955–74.
Gringarten AC. Reservoir lifetime and heat recovery factor in geothermal aquifers used for urban heating. Pure Appl Geophys. 1978;117(1–2):297–308.
Kim J, Lee Y, Yoon WS, Jeon JS, Koo M-H, Keehm Y. Numerical modelling of aquifer thermal energy storage system. Energy. 2010;35:4955–65.
Mahler A, Magtengaard J. Country update report for Denmark. In: Proceedings world geothermal congress 2010, Bali, Indonesia. 2010.
Major M. Numerical modelling of heat recovery and storage potential in deep geothermal reservoirs. Unpublished master's thesis, Aarhus University. 2016.
Mathiesen A, Kristensen L, Bidstrup T, Nielsen LH. Evaluation of the geothermal potential in Denmark. In: Geological Survey of Denmark and Greenland Report 59, In Danish. 2009.
Molz FJ, Warman JC, Jones TE. Aquifer storage of heated water: part 1—a field experiment. Groundwater. 1978;16(4):234–41.
Phillips SL, Igbene A, Fair JA, Ozbek H, Tavana M. A technical databook for geothermal energy utilization. Berkeley: Lawrence Berkeley Laboratory, University of California; 1981. p. 94720.
Poulsen SE, Balling N, Nielsen SB. Parametric study of the thermal recharge of low enthalpy geothermal reservoirs. Geothermics. 2015;53:464–78.
REN21. Renewables 2017 Global Status Report, Paris: REN21 Secretariat ISBN 978-3-9818107-6-9. 2017.
Robertson EC. Thermal properties of rock. In: Open-File Report 88-441, United States Geological Survey (USGS). 1988.
Røgen B, Ditlefsen C, Vangkilde-Pedersen T, Nielsen LH, Mahler A. Geothermal energy use, 2015 country update for Denmark. In: Proceedings world geothermal congress 2015. Melbourne: International Geothermal Association; 2015. p. 11.
Sanner B, Kabus F, Seibt P, Bartels J. Underground thermal energy storage for the German Parliament in Berlin, system concept and operational experiences. In: Proceedings world geothermal congress 2005, Antalya, Turkey, 24–29 April 2005.
Schout G, Drijver B, Gutierrez-Neri M, Schotting R. Analysis of recovery efficiency in high-temperature aquifer thermal energy storage: a Rayleigh-based method. Hydrogeol J. 2014;22:281–91. https://doi.org/10.1007/s10040-013-1050-8.
Schwartz FW, Zhang H. Fundamentals of ground water. 1st ed. New York: Wiley; 2003. p. 592.
Sommer WT, Doornenbal PJ, Drijver BC, van Gaans PFM, Leusbrock I, Grotenhuis JTC, Rijnaarts HHM. Thermal performance and heat transport in aquifer thermal energy storage. Hydrogeol J. 2014;22:263–79. https://doi.org/10.1007/s10040-013-1066-0.

Tordrup KW, Poulsen SE, Bjørn H. An improved method for upscaling borehole thermal energy storage using inverse finite element modelling. Renew Energy. 2016;105:13–21.
Voss CI, Provost AM. SUTRA a model for saturated–unsaturated variable- density ground-water flow with solute or energy transport. In: US geological survey water-resources investigations report 02-4231:250. 2003.
Welsch B, Rühaak W, Schulte DO, Bär K, Homuth S, Sass I. A comparative study of medium deep borehole thermal energy storage systems using numerical modelling. In: Proceedings world geothermal congress 2015, Melbourne, Australia, 19–25 April 2015.